Chapter 5
Silicate Liquid Immiscibility in Layered Intrusions

Ilya V. Veksler and Bernard Charlier

Abstract More and more evidence for the development of silicate liquid immiscibility during cooling of magmas in layered intrusions have been presented. Here, we review some theoretical principles with a focus on the separation of two silicate melts, i.e. silica-rich vs. iron-rich. We discuss the role of melt structure and present phase equilibria relevant to stable and metastable immiscibility. The understanding of immiscibility in magmas has strongly benefited from recent progress in experimental approaches. Kinetics studies evidence the importance of nucleation barriers in producing unmixing, coarsening and potential separation of equilibrium melts. Improvement of analytical tools has also enabled detailed study of major and trace element partitioning. The study of immiscible emulsion in volcanic rocks also brings important information on the evolution of plutonic systems and on the potential formation of compositional gap along liquid lines of descent. We then present the most recent evidence for immiscibility in some major layered intrusions, i.e. the Skaergaard, Sept Iles, intrusions of the Emeishan province, and the Bushveld complex. Paired melts are identified as contrasted melt inclusions trapped in apatite and their segregation can be responsible for the formation of Fe–Ti–P-rich rocks. We finally discuss more broadly the potential effect of immiscibility in interstitial melt and the implications on the evolution of the crystal mush.

Keywords Unmixing · Binodal · Skaergaard · Sept Iles · Bushveld

I. V. Veksler (✉)
Department of Mineralogy and Petrology, Technical University Berlin,
Ackerstrasse 74, 13355 Berlin, Germany
e-mail: veksler@gfz-potsdam.de

Department of Geology, Perm State University, Bukireva 15, Perm, Russia, 614990

B. Charlier
Department of Earth, Atmospheric and Planetary Sciences, Massachusetts Institute
of Technology, Cambridge, MA 02139, USA
e-mail: b.charlier@ulg.ac.be

Department of Geology, University of Liège, 4000 Sart Tilman, Belgium

B. Charlier et al. (eds.), *Layered Intrusions,* Springer Geology,
DOI 10.1007/978-94-017-9652-1_5

Introduction

Popular views on the significance and petrogenetic role of silicate liquid immiscibility have changed several times since the start of modern igneous petrology, from early enthusiasm (Daly 1914) to scepticism (Greig 1927; Bowen 1928) and to revived interest (De 1974; McBirney and Nakamura 1974; Philpotts 1979, 1982; Dixon and Rutherford 1979; Roedder 1979). Igneous petrologists have stumbled upon traces of liquid immiscibility in lavas and plutonic rocks sometimes by serendipity as, for example, described by Roedder (1978) who discovered glassy immiscibility products in samples of lunar basalts while trying to find hydrous fluid inclusions in olivine and plagioclase phenocrysts. Referring to another fairy tale, one could call liquid immiscibility Cinderella of igneous petrology as it is not getting proper recognition despite numerous glass and crystal "slippers" left behind in magmatic rocks. Recent years have seen a new wave of interest and significant progress in experimental and petrographic studies of silicate liquid immiscibility and its magmatic products. Hopefully, this will be the last major change of fortunes and immiscibility will hold a proper place among important magma differentiation processes.

It is believed that immiscibility between silicate melts and molten Fe–Ni alloys was responsible for the global, first-order planetary differentiation, which resulted in the formation of metal core and silicate shell during accretion of the Earth and other Earth-like planets. Immiscibility between salt, sulfide and silicate melts probably leads to formation of some types of carbonatites and magmatic sulfide deposits. Immiscibility between the drastically different chemical types of magmatic liquids has been reviewed elsewhere (e.g. Veksler 2004; Thompson et al. 2007) and is not discussed in this chapter. Here we consider only immiscibility between a pair of silicate melts. This restriction also excludes from our consideration hypothetical, essentially silica-free apatite-magnetite-ilmenite and apatite-magnetite-sulfide immiscible melts, which may have been responsible for the formation of nelsonites and Kiruna-type ore deposits in massif anorthosites and some layered intrusions (e.g., Philpotts 1967; Kolker 1982; Duchesne 1999; Hou et al. 2011).

In this chapter we briefly cover the progress since the last major reviews of the late 1970s and early 1980s (Roedder 1978, 1979; Philpotts 1979, 1982). The emphasis of this review is on layered intrusions because they are the topic of this book, and also because plutonic environment is especially favorable for full development of immiscibility and liquid-liquid fractionation. We first review some theoretical backgrounds on melt structure, phase equilibria, kinetics, and element partitioning. Separate sections deal with intrusions where the studies of immiscibility have been most extensive. We finally discuss more broadly the potential effect of immiscibility in the crystal mush.

Theoretical Principles and Definitions

Liquid Immiscibility at the Atomic Level

Liquid phases do not have long-range ordering on the atomic and molecular scale and therefore have much greater structural tolerance than crystalline solid solutions. Immiscibility in the liquid state usually occurs when the conjugate phases fundamentally differ in the type of chemical bonds. Therefore, immiscible fluid phases can be classified by their dominant types of bonding: ionic, covalent, metallic or intermolecular. Silicate melts are characterized by interplay of covalent and ionic bonds between components and they are correspondingly poorly miscible with liquids having metallic bonding (molten metals and sulphide melts) and fully dissociated ionic and molecular liquids (molten salts and supercritical C–O–H fluids).

Silicate liquid immiscibility is rooted in fundamental properties of silicate melts and highlights the distinction between two types of components, network formers and network modifiers. Network formers are small, highly-charged cations having, because of the small size, coordination numbers no greater than 4 in melts, glasses and crystalline silicates. Four-fold coordinated Si^{4+} is the most abundant and important network former of natural magmas. The group of network-formers in natural and technological melts also includes P^{5+}, B^{3+} and some other cations, which in nature are usually present only in trace amounts (e.g. Ge^{4+}, Sb^{3+} and As^{3+}).

Network-modifying cations have ionic radii greater than 87.2 pm and coordination numbers equal to, or higher than 5 (Hudon and Baker 2002). The group comprises alkali and alkaline earth cations excluding Li^{+}, Be^{2+} and Mg^{2+}, REE cations, Th^{4+} and U^{4+}. Cations with ionic radii greater than Si^{4+} (26 pm) but smaller than 87.2 pm belong to the amphoteric group. According to spectroscopic studies, amphoteric cations have at least two coordination numbers. One coordination number is four and another one is usually five or six (see Hudon and Baker 2002 for details). The most important amphoteric cation of natural magmatic melts is Al^{3+} and the group also includes Li^{+}, Be^{2+}, Mg^{2+}, Mn^{2+}, Zn^{2+}, Sc^{3+}, Ga^{3+}, Ti^{4+}, Zr^{4+}, Hf^{4+}, Nb^{5+}, Ta^{5+} and some other high field strength cations.

It has been noticed since long ago (see review of earlier works by Hess 1995) that the size of miscibility gaps in binary metal oxide—silica systems MO–SiO_2 correlate with Coulombic properties of the metal cations, such as ionic potential. Ionic potential is the ratio of Z/r, where Z is the nominal charge and r is the atomic radius of the cation. The correlation is especially evident in the binaries of alkali and alkaline earth cations (Fig. 5.1). To rationalize the correlation, Hess (1995, 1996) proposed that the forces responsible for melt unmixing at the atomic level are Coulombic and repulsive in nature. He pointed out that network-modifying cations are surrounded in silicate melts by both bridging and non-bridging oxyanions. Oxygen ions in bridging (Si–O–Si) and non-bridging positions (Si–O—M, where M is a network-modifying cation) isolate the network-modifier cations from each other by providing screens that mask the positive charges. However, modifier cations that are partly or wholly coordinated by bridging oxygen are poorly shielded from

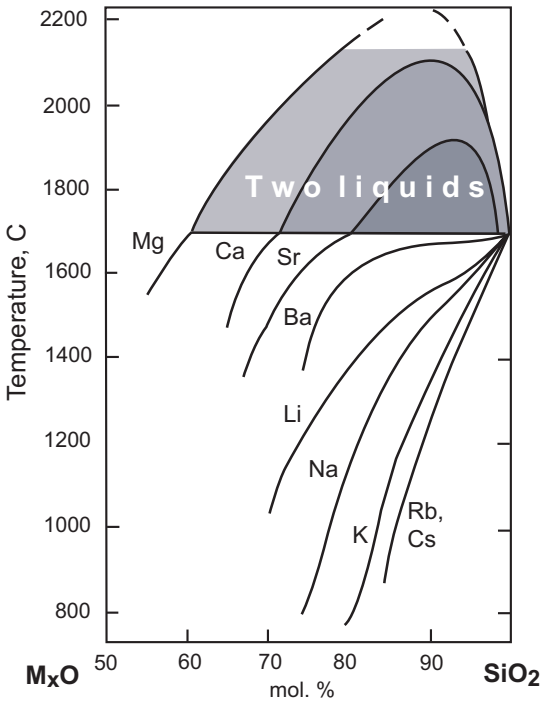

Fig. 5.1 Silica-rich portions of alkali and alkaline earth oxides binaries with two liquid fields (after Levin et al. 1964)

each other because the bridging oxygen ions are bonded to Si^{4+} cations by strong covalent bonds. Consequently, significant Coulombic repulsions build up between network-modifying cations, and they may eventually result in melt unmixing and phase separation. The higher the ionic potential of modifier cations, the greater are the Coulombic repulsions between them, and the larger is the width of the resulting miscibility gap.

In a detailed analysis of binary systems, Hudon and Baker (2002) noticed that the relationships between the ionic potential of network-modifying cations and the size of miscibility gaps are not linear. Furthermore, each group of homovalent cations (cations with the same *Z*) forms its own trend. For each group, the compositional width of miscibility gap and the unmixing temperature increase with *Z*/*r*, reach a maximum and then decrease. The maximum is reached at $r = 87.2$ pm, which, as mentioned above, defines the transition from true network modifiers to amphoteric cations. The authors proposed the existence of structural control on immiscibility in which the cation radius appears to have an important role. To rationalize the convex trends, they pointed out the increasing degree of covalency of the M–O bonds in homovalent groups of elements with decreasing *r*. Therefore, amphoteric cations capable of 4-fold coordination seem to undergo weak or no Coulombic repulsion and tend to produce little or no phase separation.

Liquid immiscibility in lunar and terrestrial magmas has been mostly observed in Fe-rich compositions and the link between immiscibility and high Fe contents has been interpreted as a consequence of specific properties of Fe cations. Cations

of transition elements from the first row in the periodic table, such as Fe^{2+}, Co^{2+}, Ni^{2+}, Cu^{2+}, V^{3+}, and Cr^{3+}, have five d-electron orbitals, which are known to poorly shield the atomic nucleus (Hudon and Baker 2002). Notably, miscibility gaps associated with the divalent cations in corresponding oxide-silica binaries are larger than expected from the general *Z/r* trend. Immiscibility gaps are even greater in binaries of trivalent Cr^{3+}, V^{3+}, and Fe^{3+} (Hudon and Baker 2002).

Binodal and Spinodal

In thermodynamic terms, liquid immiscibility is linked with variations of the Gibbs free energy of mixing *G* with composition *X* at constant pressure and temperature (Fig. 5.2a). Detailed discussions of free energy in relation to immiscibility can be found in numerous reviews and textbooks (e.g. James 1975; Doremus 1994; Shelby 2005). The simplest case is that of a binary liquid where free energy varies smoothly with composition in the whole range between pure components A and B (Fig. 5.2a). Here the *G-X* curve is characterized in the region of unmixing by a local maximum. Tangent points *a* and *b* of the common tangent line define the compositions of the equilibrium immiscible liquids L_a and L_b. In the compositional interval between L_a and L_b a single homogenous liquid has a higher free energy than a mixture of the two immiscible liquids. Thus the two-liquid phase assemblage is the thermodynamically stable one, whereas the *a-b* segment of the *G-X* curve is metastable. The compositions L_a and L_b depend on temperature, and the loci of points *a* and *b* define a *T-X* curve that is termed binodal (Fig. 5.2b). All dry immiscible silicate systems known to date are characterized by convex binodals with upper consolute (or critical solution) points, at which the distinction between coexisting liquid phases vanishes. Some researchers (Navrotsky 1992; Hess 1996) have proposed that concave binodals and lower consolute points may also exist. At the consolute points liquids undergo second order (continuous) phase transition. As they approach this transition with falling temperature they pass through a region of critical opalescence (Fig. 5.2b). This region is the site of anomalously large compositional fluctuations and abnormal variations of viscosity, density, compressibility, and other physical properties (Simmons et al. 1970; Simmons and Macedo 1971; Mazurin and Porai-Koshits 1984). Similarly, the loci of inflexion points s_1 and s_2 in the *G-X* curves (Fig. 5.2a) where the second derivative $(\delta^2 G/\delta x^2)_{T,P}=0$ defines the spinodal (Fig. 5.2b). The importance of both the spinodal and the phenomenon of critical opalescence in the understanding of the mechanism of liquid unmixing will be considered below.

Stable and Metastable Immiscibility

With regards to relationships between liquid immiscibility and crystallization, two topological cases are possible. In the first case, a stable two-liquid field emerges in

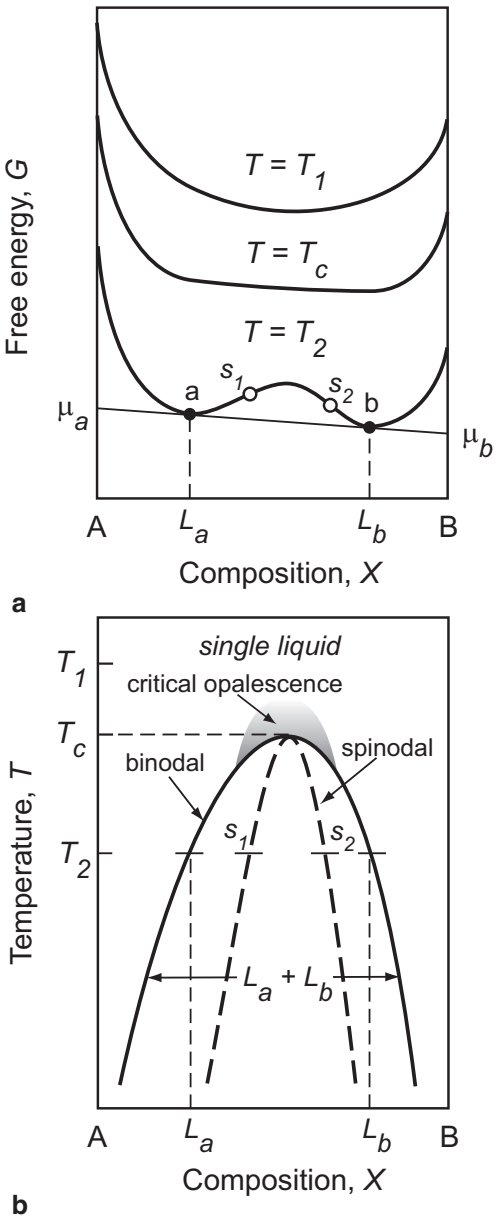

Fig. 5.2 Binodal and spinodal in a schematic binary *A–B*. **a** Gibbs free energy (*G*) versus composition (*X*) curves for temperature T_1 above the consolute point, the consolute temperature T_c, and temperature T_2 below the consolute point. Immiscible liquids *a* and *b* lie on a common tangent line to the energy curve. X_a and X_b are equilibrium compositions; μ_a and μ_b are chemical potentials of the components *A* and *B*. Inflexion points s_1 and s_2 define the spinodal. **b** Two-liquid region *a* + *b*, binodal and spinodal in *T*-*X* coordinates. T_1, T_c and T_2 are the same as in plot a. *Shaded area* shows a region of critical opalescence

a region where segments of the binodal dome overlie the liquidus surface. One or more crystalline phases may coexist with two immiscible liquids at the intersections between the binodal and the liquidus. In the second case, the binodal may be completely submerged (i.e. subliquidus), and in that case liquid immiscibility

is metastable. These two types of relationships are schematically illustrated for a binary system in Fig. 5.3. The systems CaO–SiO_2 and BaO–SiO_2 (Fig. 5.1) serve as examples of the stable and metastable cases, respectively (Greig 1927; Hudon and Baker 2002). In *T-x* diagrams, the liquidus is flattened above the metastable binodal,

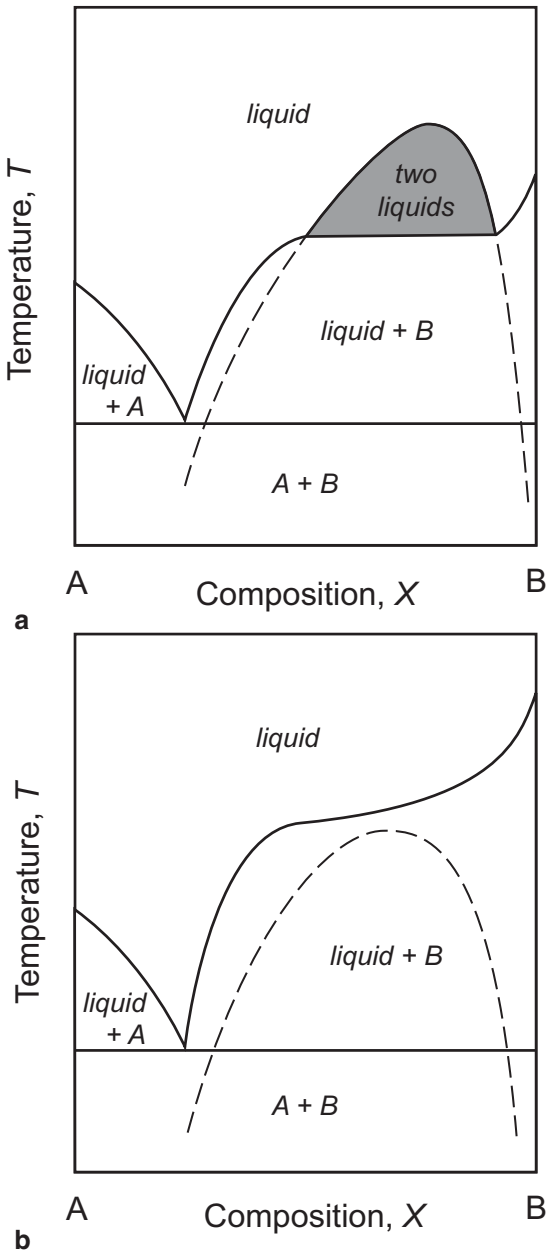

Fig. 5.3 Schematic binary phase diagrams showing **a** stable two-liquid field (*shaded area*) with its metastable extention (*dashed curves*) and **b** entirely sub-liquidus metastable immiscibility

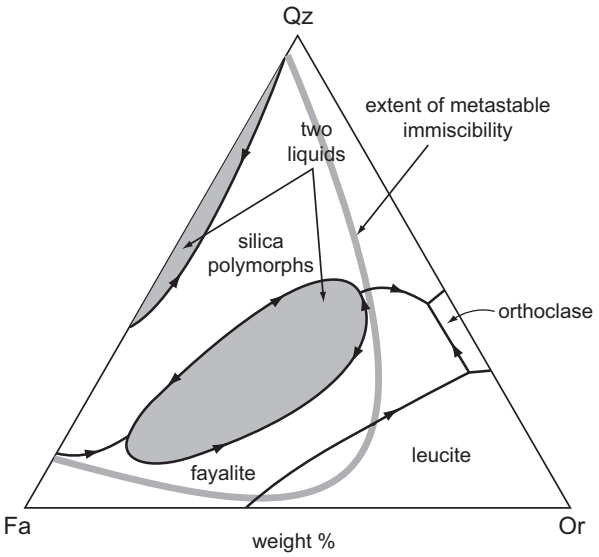

Fig 5.4 Liquid immiscibility in the fayalite *Fa*—orthoclase *Or*—silica *Qz* pseudo-ternary join after Roedder (1951, 1978). *Solid grey curve* shows the extent of sub-liquidus immiscibility according to Visser and Koster van Groos (1979)

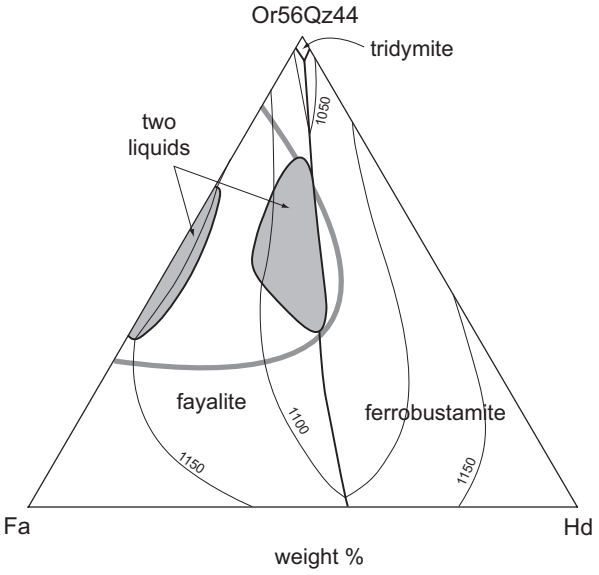

Fig. 5.5 Phase diagram of the join fayalite (*Fa*)—hedenbergite (*Hd*)—orthoclase (*Or*)—silica (*Qz*) after Hoover and Irvine (1978) showing fields of liquid immiscibility (*shaded areas*), cotectics and isotherms 1050, 1100 and 1150 °C. *Solid grey curve* shows the extent of two-liquid field in compositions containing 1.7–1.8 P_2O_5 according to Bogaerts and Schmidt (2006)

exhibiting a characteristic sigmoidal shape (Fig. 5.3b). Similar relationships are known in many ternaries and pseudo-ternaries, and some examples are presented in Figs. 5.4 and 5.5. It follows from Figs. 5.4 and 5.5 that seemingly separate stable miscibility gaps in multicomponent systems may actually represent fragments of a single binodal surface.

Nucleation Barriers

In the framework of currently accepted kinetic models (James 1975; Mazurin and Porai-Koshits 1984; Shelby 2005 and references therein), liquid immiscibility in compositional regions between the binodal and spinodal proceeds via nucleation and growth. It thus follows that they may be hampered by the thermodynamics and kinetics associated with nucleation and growth. The origins of thermodynamic barriers can be explained using the same *G*-*X* curve as introduced in Fig. 5.2a, and the relationships are illustrated in Fig. 5.6 following James (1975). For the bulk composition *x* lying between points *a* (binodal), and s_1 (spinodal), the overall free energy decrease due to unmixing to equilibrium liquids *a* and *b* (excluding interfacial effects) graphically corresponds to the vertical segment ΔG between the free energy curve at composition *b* and the tangent drawn to the curve at the composition *x*. This energy drop is the driving force for separation of the equilibrium phases. It should be noted however that when phase separation develops in a nucleation and growth regime, small sub-critical compositional fluctuations (represented for example, by composition *f*) will produce an increase in free energy (the segment Δg). This increase represents a thermodynamic barrier for unmixing. Clearly a fluctuation must develop beyond the composition *e* before the free energy starts to decrease, and the barrier is overcome. Thus, in nucleation region, the system is metastable with respect to infinitesimal compositional fluctuations. In contrast, there is no thermodynamic barrier for phase separation within the spinodal region between the inflection points s_1 and s_2 as the free energy change is negative for an infinitesimal fluctuation. Nonetheless, kinetic limitations on phase separation are universal. These limitations exist regardless of the exact mechanism of phase separation or the position of initial

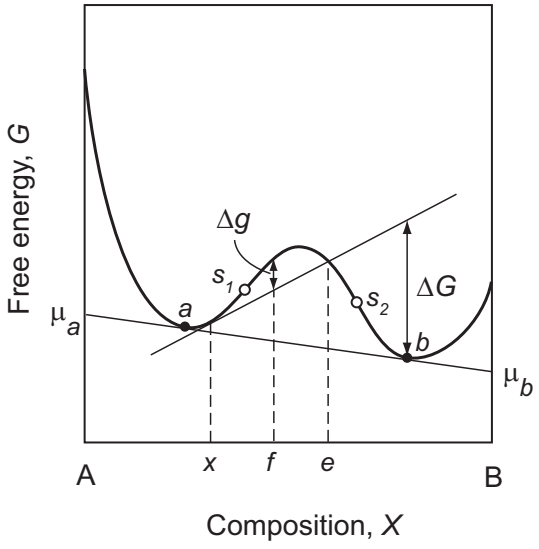

Fig. 5.6 Free energy (*G*) *vs*. composition (*X*) diagram showing graphical method of determining the thermodynamic driving force and the barrier for liquid-liquid phase separation. See text for details

composition x, because they arise from material transport and dynamic parameters, such as diffusion rates and viscosity.

Recent Progress in Experimental Studies

Magma Evolution Paths and Immiscibility Region

With the exception of rare cases of strongly overheated impact melts (e.g. the parental magma of the Sudbury complex right after the impact) terrestrial magmas are produced by partial melting of mantle or crustal rocks and therefore are crystal-saturated. The liquid line of descent and thus the potential for silicate melts to reach a two-liquid field is controlled by solid phases crystallization with decreasing temperature and their effect on the composition of residual melts. In dry systems, extreme iron enrichment (> 18–19 wt.% FeO) was usually considered as necessary for the onset of unmixing (Dixon and Rutherford 1979; Philpotts and Doyle 1983). This is easily accomplished in alkali-poor systems such as lunar rocks or eucrites (Rutherford et al. 1974; Powell et al. 1980), but alkali-rich liquids evolve ultimately to iron depletion and silica enrichment (Veksler 2009). However, as illustrated by the experimental study of Charlier and Grove (2012), immiscibility can also develop along the liquid line of descent during the iron depletion and silica enrichment that occurs after Fe–Ti oxides appear in the crystallizing assemblage. The liquid line of descent must reach the appropriate compositional field to unmix, but the other condition is that the liquidus temperature crosses a super-liquidus binodal during differentiation (Fig. 5.7). Two classical study of the evolution of tholeiitic basalts by Juster et al. (1989) for the Galapagos spreading center and by Toplis and Carroll (1995) for the parental magma of the Skaergaard layered intrusion did not satisfy this condition.

In ternary systems and systems with greater number of components, stable immiscibility domes can sit either above cotectics (like, for example in the Roedder system illustrated in Fig. 5.4) or a dome may be positioned above a thermal divide (Fig. 5.8). In the first case, mechanical separation of immiscible melts does not change the liquid line of descent and the general direction of system evolution. In the Roedder system, both melts eventually follow the fayalite-silica, or (at higher fO_2) magnetite-silica cotectics and end up in the same eutectic with orthoclase. In some ternaries (e.g. $CaO–B_2O_3–SiO_2$) immiscibilty domes sit on top of thermal divides and mechanically separated immiscible melts evolve by further crystallization in different directions. The topology of natural multicomponent ferrobasaltic-andesitic systems is very complex but it seems that at low pressure, when plagioclase is stable and forms a thermal divide, the situation corresponds to the second case. That is, mechanically separated Fe-rich melt would probably further evolve along the “Fenner” Fe-enrichment trend ending in a Fe-rich eutectic, whereas the silica-rich liquid follows a more familiar Bowen trend of further silica enrichment, all the way down to the granitic eutectic.

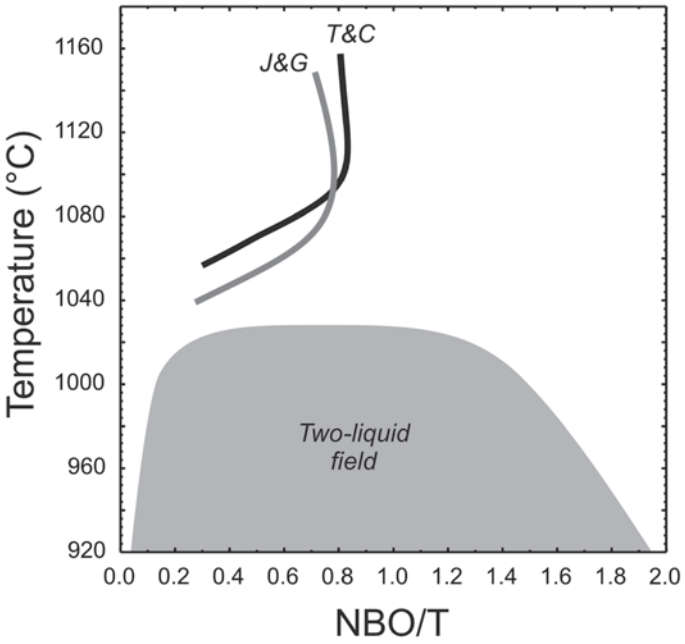

Fig. 5.7 Temperature as a function of the degree of polymerization (NBO/T) of experimental melts. The *grey* area represents the maximum compositional space of the two-liquid field from Charlier and Grove (2012). Liquid lines of descent of Toplis and Carroll (1995) (*T&C*; *black*) and Juster et al. (1989) (*J&G*; *grey*) are plotted

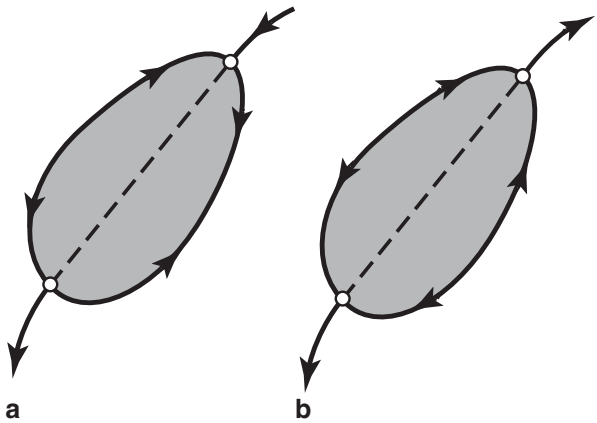

Fig. 5.8 Two topological types of liquid immiscibility regions in relationship to liquidus surface. **a** On top of a cotectic. **b** On top of a thermal barrier

Silicate liquid immiscibility is difficult to identify also because it can be a furtive agent of fractionation (Longhi 1998). Indeed, a melt entering a two-liquid field upon cooling can leave this field because of crystallization and compositional evolution of the bulk residual liquid. This is schematically illustrated on Fig. 5.9 in

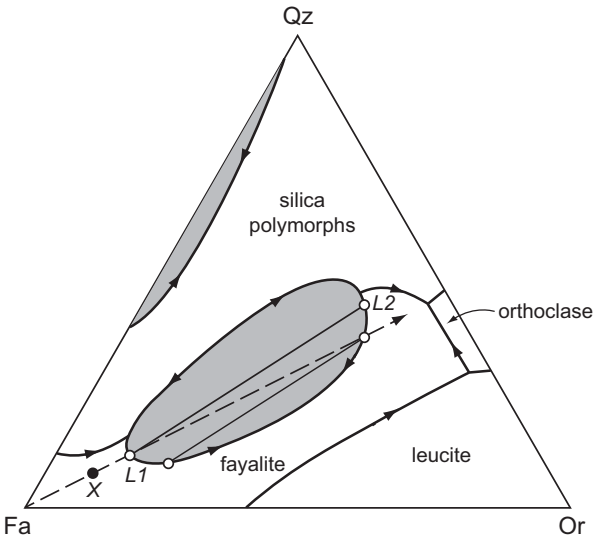

Fig. 5.9 Illustration of a crystallization path for liquid composition X in the fayalite (*Fa*)—orthoclase (*Or*)—silica (*Qz*) pseudo-ternary join after Roedder (1951, 1978), showing the furtive nature of liquid immiscibility upon cooling. *Grey* areas are fields of stable immiscibility. See text for discussion

the fayalite (Fa)—orthoclase (Or)—silica (Qz) pseudo-ternary with the equilibrium crystallization trend for liquid *X*. Liquid *X* located in the stability field of fayalite crystallizes this phase until it reaches the two liquid field, marking the separation of a high-silica liquid *L2*. The paired low-silica liquid *L1* reacts with crystallizing fayalite to produce the high-silica liquid. As the reaction proceeds upon cooling, compositions of the two liquids move closer together, and when a line from the high-silica liquid to fayalite passes through the bulk composition (*X*), the last of the low-silica liquid is consumed and the high-silica liquid moves directly away from fayalite in the one-liquid stability field (Longhi 1998). Thus, after complete solidification of the system, there is no remaining trace of silicate liquid immiscibility. The high-silica liquid produced ultimately has only recorded the fractionation of fayalite, K-feldspar, and silica at the eutectic.

In the Sept Iles layered intrusion (see Section “Sept Iles”), immiscibility has been interpreted to be a passing phenomenon limited to a narrow temperature interval, evaluated to be between 1015 and 985 °C (Charlier et al. 2011; Namur et al. 2012, 2015). Both immiscible melts evolved along the binodal upon cooling, forming cumulate rocks with identical mineral compositions but contrasted mineral modes. The bulk liquid composition was evolving towards silica-enrichment and iron-depletion by fractional crystallization to eventually leave the two-liquid field. Immiscibility had thus no influence on the liquid line of descent, except for the absence of intermediate melts.

Liquid-Liquid Element and Isotope Partitioning

Major and Trace Elements

Our knowledge of element partitioning between immiscible silicate melts has greatly improved in recent years owing to the introduction of new experimental and analytical methods such as high-temperature centrifuge separation (Schmidt et al. 2006; Veksler et al. 2006) and laser ablation ICP-MS analyses. It is now possible to analyze dozens of elements at concentrations varying over several orders of magnitude in the same sample and even at the same spot. Therefore, comparisons between individual elements and/or different chemical groups can be done with greater confidence.

The general picture that emerges from recent studies implies close links between ionic properties (e.g. the nominal charge Z and ionic radius r combined in the form of ionic potential Z/r) and liquid-liquid distribution of an element, which is usually expressed in the form of Nernst distribution coefficient $D_i = C_i^{Lfe}/C_i^{Lsi}$ where C's are weight concentrations, subscripts denote the element and superscripts denote phases (*Lfe*—Fe-rich melt; *Lsi*—silica-rich melt). The connection is hardly surprising in view that Coulombic interactions appear to be the principal driving force for silicate liquid immiscibility at the atomic level (see Section "Liquid Immiscibility at the Atomic Level"). Liquid-liquid D values closely correlate with the widths and consolute temperatures of miscibility gaps in corresponding metal oxide-silica binaries (Hudon and Baker 2002; Schmidt et al. 2006; Veksler et al. 2006). Elements, with broader miscibility gaps in the binaries with silica tend to have higher D values and stronger concentrate in the silica-poor, Fe-rich conjugate liquid. When plotted against ionic potential Z/r, liquid-liquid D values of isovalent elements tend to form convex trends similar to those described by Hudon and Baker (2002) for the consolute temperatures.

A typical plot of the liquid-liquid D values against Z/r is presented in Fig. 5.10. Only three trace elements out of 37 shown on the plot, together with the major components K, Al and Si, concentrate in the silica-rich liquid. The elements include network modifiers with the lowest ionic potentials (Cs and Rb) and a network former Sb. The highest D values are reached by REE and trivalent transition elements Cr and V. Absolute D values vary with temperature, redox conditions and melt chemistry but the general pattern of element partitioning and proportionality between the D values of individual elements hold. On the basis of experimental data, Schmidt et al. (2006) proposed a modified regular solution model, which allows to calculate D_M of a trace element M in multicomponent compositions from the width of miscibility gap expressed as X_{FeO}^{Lfe}—X_{FeO}^{Lsi} and the consolute temperature of the binodal in the $MO–SiO_2$ binary.

Oxygen Isotopes

Kyser et al. (1998) and Lester et al. (2013b) studied oxygen isotope partitioning between Fe- and Si-rich immiscible liquids in the system $K_2O–FeO–Fe_2O_3–Al_2O_3–SiO_2$ at the atmospheric pressure and 1180 °C, and in similar compositions

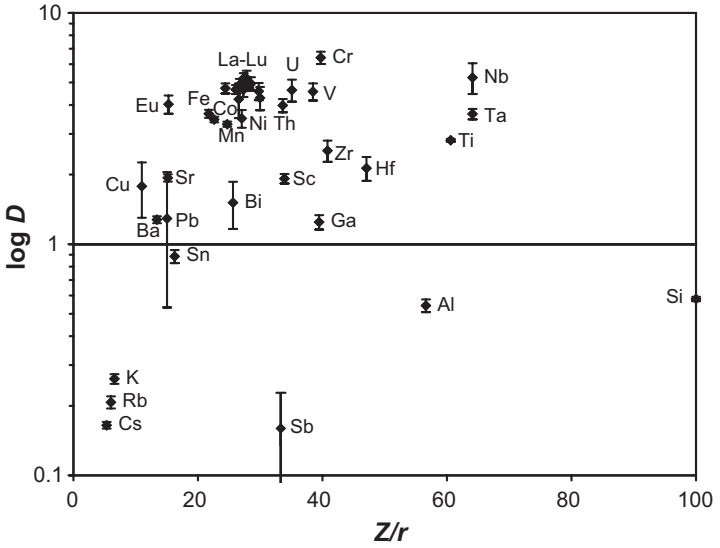

Fig. 5.10 Liquid-liquid Nernst partition coefficients *D* plotted against ionic potential *Z/r*. average values with standard deviations (shown as *vertical bars*) for a series of experiments on synthetic compositions in the system K_2O–FeO–Fe_2O_3–Al_2O_3–SiO_2 at 1200 °C and log fO_2 between −8.3 and −8.7 (Veksler unpublished data)

doped with H_2O, P and S at 1100–1200 °C and 200 MPa. In both studies Si-rich liquids were found to have $\delta^{18}O$ values higher than those of the Fe-rich liquids by 0.4–1 ‰. The observed preferential partitioning of ^{18}O into the Si-rich liquid is consistent with crystal-melt oxygen isotope equilibria and oxygen isotope fractionation in Soret (thermal) diffusion experiments. In all the cases, crystallochemical principles seem to work in the same way and phases or liquid fractions with more polymerized structure tend to be enriched in ^{18}O.

The Kinetics of Liquid Immiscibility

It has been recognized that silicate melts with compositions in vicinity of miscibility gaps often quench to opalescent glasses showing heterogeneity at sub-micron scale. Correct interpretation of sub-micron exsolutions in the glasses is crucial for distinguishing between stable and metastable immiscibility (see Section “Stable and Metastable Immiscibility”) and requires good knowledge of the kinetics of liquid immiscibility. Kinetic issues were at the core of the discussion about the actual extent of the stable miscibility gap in the system K_2O–FeO–Al_2O_3–SiO_2 (Visser and Koster van Groos 1976, 1977; Freestone and Hamilton 1977; Roedder 1978) and in multicomponent compositions used in centrifuge experiments (Veksler et al. 2007,

2008a, b; Philpotts 2008). Two alternative views have been formulated. First is that the fine heterogeneity in glasses is due to instant melt unmixing during quenching. In other words, melt was homogenous before quenching and unmixed when temperature dropped below the metastable segment of the binodal (Fig. 5.3) but was still above the glass transition temperature. Second interpretation of the turbid, opalescent glasses is that they form from melts, which were heterogeneous before quench and represented thermodynamically stable but slowly growing sub-micron emulsions.

The mechanisms for melt unmixing and kinetics of droplet nucleation and growth have been studied extensively in technological melts and glasses (James 1975; Mazurin and Porai-Koshits 1984). In a typical case, initial nucleation of nanometer-sized immiscible droplets is believed to be very fast and further growth is dominated by process of coarsening, which is termed Ostwald ripening. Ripening is preferential growth of larger droplets at the expense of smaller ones driven by overall decrease in interfacial free energy γ. Theoretical models of the coarsening stage predict that the average droplet radius r should increase proportionately either to the square root or the cubic root of time (e.g. see review by James 1975). The exact relationship depends on the degree of super-saturation, and is also determined by the process that controls the growth (long range diffusion *versus* surface reaction rate). In any case, coarsening is faster when the value of γ is high.

First experimental measurements of interfacial tension γ have been recently carried out for immiscible Fe-rich and silica-rich melts in the system K_2O–FeO–Fe_2O_3–Al_2O_3–SiO_2 (Veksler et al. 2010). The measurements were performed in air for the most oxidized and chemically contrasting melt compositions. The measured γ values in the range of 8–16 mN/m are very low. For comparison with more familiar examples, γ values between water and immiscible organic liquids, such as mineral oil, benzene, or purified vegetable oils vary at room temperature between 30 and 50 mN/m. Veksler et al. (2010) pointed out that γ values for natural, less compositionally contrasting ferrobasaltic and rhyolitic melts should be even lower by a factor of 2 or 3. In the context of kinetic theories of liquid immiscibility (James 1975), low interfacial tension implies easier nucleation, higher nucleation density but, on the other hand, slow coarsening of the droplets by Ostwald ripening and protracted stability of fine emulsions.

The kinetics of silicate liquid immiscibility in natural magmas has been studied only briefly (Martin and Kushiro 1991) and its experimental coverage remains insufficient. In view of recent kinetic studies by Veksler et al. (2008a, 2010), silicate liquid immiscibility in natural ferrobasaltic, andesitic or rhyolitic magmas is likely to produce very fine, possibly sub-micrometer emulsions that may be stable over considerable time, and have significant effects on magma dynamics. Slow coarsening of the emulsions should hamper gravitational separation of immiscible melts, and may be among the reasons why traces of immiscibility are usually hard to detect in partly or fully crystallized igneous rocks.

The effects of H_2O and Other Volatile Components on Liquid Immiscibility

Lester et al. (2013a) studied the effects of H_2O, S, P, Cl and F additions on liquid immiscibility in the system K_2O–FeO–Fe_2O_3–Al_2O_3–SiO_2. The additions of H_2O at 200 MPa were shown to dramatically suppress liquidus surface temperatures, expand the stability field of magnetite and decrease that of silica minerals, thereby increasing the *T–X* range of the miscibility gap. Thus, the composition range of the miscibility gap at the fO_2 level of the magnetite-hematite (MH) buffer is increased relative to the range in equivalent anhydrous melts. At fO_2 equivalent to the Ni–NiO buffer H_2O addition displaced the miscibility gap to more silica-rich compositions and presumably extends the two-liquid field. Sulfur and phosphorus were shown to further expand the miscibility gap. Three-liquid immiscibility between Fe-rich silicate liquid, a Si-rich silicate liquid and a Fe-sulfide liquid was observed in some hydrated compositions at fO_2 = MH.

Silicate Liquid Immiscibility in Magmatic Systems

Volcanic Systems and the Daly Gap

Most mantle-derived lavas and pyroclastic materials erupt at the surface after extensive differentiation in magma chambers at depth. Volcanic products, which can be viewed as spills and overflows from intrusive systems, carry important information about magma evolution in the process of magma transformation into a layered intrusion. Therefore, microscopic and macroscopic evidence of liquid immiscibility in volcanic rocks is relevant for the present discussion.

Immiscible droplets of glasses trapped in the mesostasis of basalts have been recognized worldwide in both tholeiitic and alkaline series (e.g. De 1974; Sato 1978; Philpotts 1982; Kontak et al. 2002; Sensarma and Palme 2013). These immiscible interstitial textures consist of brown spheres, usually smaller than 10 μm, enclosed in a silica-rich glass. Dark globules are commonly finely crystallized to Fe–Ti oxides, iron-rich pyroxene and other fine-grained material whereas the glassy texture of the silica-rich component is better preserved. Examples of immiscibility textures in volcanic rocks are presented in Fig. 5.11.

Evidence for unmixing provided by these small-scale textures is usually not considered as sufficient to support the potential role of immiscibility as a large-scale differentiation process along the basalt-rhyolite evolution trend. However, an implication of silicate liquid immiscibility is that compositions between unmixed pairs cannot exist as homogeneous melt. Indeed, when a liquid line of descent of homogeneous melts reach a binodal surface, two contrasting liquids are produced. This is responsible for a gap of intermediate homogeneous melts during further cooling and differentiation. This absence of intermediate compositions is a major characteristic

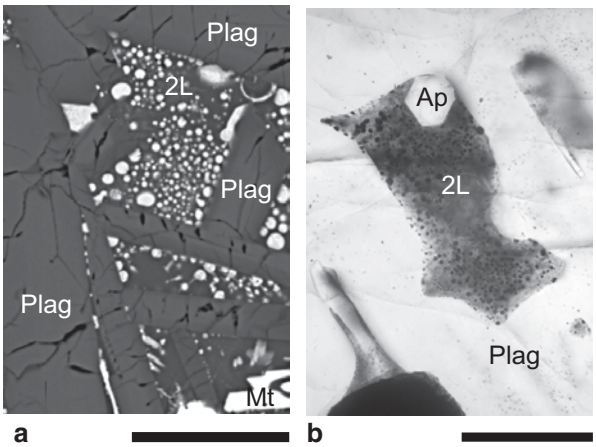

Fig. 5.11 Immiscibility textures in volcanic rocks. **a** Fe-rich droplets in silicic glass in mesostasis of tholeitic picrite from Koolau, Hawaii. Back scattered electron image. **b** Immiscible melt inclusions (*black* Fe-rich droplets in transparent silicic glass) in plagioclase phenocrysts in basaltic andesite from Mull, Scotland. Apatite crystal was trapped with the melt inclusion. Optical transmitted *light* image. Scale bars correspond to 50 microns. Abbreviations for phases: *Ap* apatite, *Plag* plagioclase, *Mt* magnetite, *2L* immiscible glasses

of tholeiitic series (Chayes 1963; Thompson 1972; Charlier et al. 2013). In the Sept Iles intrusive suite (see Section "Sept Iles"), silicate liquid immiscibility has been invoked to explain the dearth of intermediate (monzodioritic) melts along the evolution from tholeiitic basalt to A-type granite (Charlier et al. 2011; Namur et al. 2011).

Immiscibility in Mafic Layered Intrusions

Skaergaard

Since the pioneering study by Wager and Deer (1939), the Skaergaard intrusion in East Greenland became a classical example of a mafic layered intrusion. General information about the intrusion can be found in numerous reviews (e.g. McBirney 1996). First evidence for silicate liquid immiscibility in the Skaergaard intrusion came from experiments on synthetic compositions modeling evolved liquid fractions of the Skaergaard magma (McBirney and Nakamura 1974). Immiscibility was observed in mixtures of Fe-rich liquids and silica-rich granophyre precipitating mineral assemblages of the Upper Zone at temperatures around 1010–1015 °C, which is no more than 10 °C above the liquidus temperature. The composition of the Fe-rich liquid was derived from partial melting experiments on natural rocks from the top of the Upper Zone (UZc) and contained 30.5 wt.% FeO_t (McBirney and Naslund 1990). Direct confirmation that immiscibility had indeed taken place in the Skaergaard intrusion was obtained in a study of melt inclusions in cumulus apatite

from the Upper Zone of the Layered Series (Jakobsen et al. 2005). Many cumulus apatite crystals in apatite-rich layers of the Upper Zone were found to contain melt inclusions of two distinct types easily recognizable under optical microscope as dark-coloured and light-coloured. Electron microprobe analyses of the inclusions showed that the compositions of the two types compared well with the Fe-rich and silica rich immiscible liquids previously produced in experiments (McBirney and Nakamura 1974) and reported as glasses in mesostasis of natural basaltic and andesitic lavas (Philpotts 1982). Therefore, the inclusions were interpreted as immiscible liquid droplets trapped by growing apatite crystals during crystallization and unmixing of the Skaergaard magma.

The discovery of the apatite-hosted melt inclusions posed further questions: (1) when exactly was magma unmixing reached at Skaergaard and (2) how much impact, if any, did immiscibility and liquid-liquid fractionation have on magma evolution? But regardless of the timing and material transport capacity, new proof of liquid immiscibility revived an old debate about the general direction of magma evolution at Skaergaard. Some researchers (Hunter and Sparks 1987, 1990; Toplis and Carroll 1995) argued in the past that the onset of magnetite and ilmenite crystallization must have turned liquid evolution in the Skaergaard magma towards silica enrichment, while others (e.g. McBirney and Naslund 1990; Thy et al. 2006) argued that Fe enrichment continued despite crystallization of Fe–Ti oxides and reached 30 wt.% FeOt. Numerous intermediate trends were proposed between the extremes (e.g. Brooks and Nielsen 1990; Morse 1990; Nielsen 2004). On the other hand, if silicate liquid immiscibility and separation of immiscible liquids by gravity played a significant role in magma differentiation not only in the Upper Zone but also earlier in the Middle Zone and at the top of the Lower Zone, liquid-liquid fractionation would account for the apparent diversity of the liquid evolution trends and finally resolve the long-lasting debate.

Veksler et al. (2007) tried to establish the exact timing of immiscibility at Skaergaard and in other examples of tholeiitic magma in a series of high-temperature centrifuge and static reverse experiments. The study revealed significant kinetic problems hampering experimental reproduction of liquid immiscibility in multicomponent system analogous to Skaergaard magma. Unmixing of a synthetic analogue of the Skaergaard parental liquid at 1110–1120 °C corresponding to the formation of the Middle Zone did not develop beyond sub-micron, nanoscale emulsions. Nevertheless, the emulsions showed signs of macroscopic separation in centrifuge experiments and were interpreted as stable, super-liquidus immiscibility. Such interpretation and geological implications of the study were challenged (McBirney 2008; Morse 2008; Philpotts 2008). In reply, Veksler et al. (2008b) admitted that experimental evidence for early magma unmixing at Skaergaard was inconclusive but stressed the importance of new petrographic observations confirming that immiscibility had played an important role in magma differentiation at Skaergaard.

Mineralogical and petrographic traces of silicate liquid immiscibility were revealed in the Skaergaard Layered Series from the top of the Lower Zone upwards by detailed studies of plagioclase zoning (Humphreys 2011), plagioclase-hosted melt inclusions (Jakobsen et al. 2011) and late-stage intercumulus reactive

microstructures including serrated grain boundaries between pyroxene and plagioclase primocrysts, olivine rims around magnetite and ilmenite crystals, fish-hook pyroxenes and mafic symplectites (Holness et al. 2011). The reactive symplectites are characterized by extensive reverse zoning of plagioclase and replacement of orthopyroxene by fayalitic olivine and ferroaugite. The reactive microstructures document significant material transport in the cumulus mush of the Layered Series, which resulted in the depletion of late-stage intercumulus liquid in alkalis and silica, and enrichment in Ca and Fe. In view of the absence of reactive symplectites from the Marginal Border Series, where effective separation of immiscible liquids by gravity was impossible, the reactive microstructures in the Layered Series were interpreted as products of gravitational liquid-liquid separation leading to late-stage replacement reactions between residual Fe-rich liquid and cumulus primocrysts.

In summary, there is very strong evidence that silicate liquid immiscibility took place in the Skaergaard intrusion and magma unmixing resulted in fractionation of macroscopic volumes of Fe-rich and silicic immiscible products between the Upper Zone of the Layered Series and the Upper Border Series. There is also little doubt that starting from the top of the Lower Zone and through the Middle Zone of the Layered Series, intercumulus crystallization at the bottom of the magma chamber differed from crystallization in the main overlying magma and at the roof of the intrusion. Strong enrichment of intercumulus liquid at the bottom in Fe oxides was accompanied by depletion in alkalis and silica, which is inconsistent with experimental phase equilibria constraints and mass balance in a closed system (Veksler 2009). Intercumulus liquid immiscibility and gravitational liquid-liquid fractionation appear to be the most viable explanation of the observed macroscopic trends and the origin of reactive microstructures in the Layered Series.

Sept Iles

The Sept Iles layered intrusion is part of an intrusive suite on the north shore of the Saint-Lawrence River (Quebec; Higgins 2005; Namur et al. 2010, 2015). The intrusion crystallized from a ferrobasaltic parent magma and is subdivided into a Layered Series of troctolite and gabbro, an anorthositic Upper Border Series and a granitic Upper Series. The liquid line of descent followed a tholeiitic trend, and the cooling of the chamber was interrupted by two major and a series of minor influxes of magma (Namur et al. 2010, 2011).

Silicate liquid immiscibility and segregation of iron-rich and silica-rich paired melts have been recognized as a major differentiation process in the Sept Iles layered intrusion (Charlier et al. 2011; Namur et al. 2012). Evidence is provided in rocks from the Critical Zone of the intrusion. This horizon contains the most evolved cumulates of the megacyclic units II. They are made up of plagioclase ($An_{55–34}$), olivine ($Fo_{66–21}$), clinopyroxene (Mg# 75–55), ilmenite, magnetite, apatite, ± pigeonite. Two independent characteristics of these rocks support they have crystallized from an emulsion of two immiscible melts: (1) contrasting melts inclusions trapped in apatite and, (2) bimodal bulk-rock compositions of ferrogabbros.

Polycrystalline melt inclusions are ubiquitously trapped in apatite of ferrogabbros from the Critical Zone (Charlier et al. 2011). Two types of inclusions are clearly distinguished and can occur in the same apatite grain: dark inclusions which contain chlorite, amphibole, plagioclase, Fe–Ti oxides and fine-grained material; and light-coloured inclusions with albite, orthoclase, biotite, amphibole, fine-grained material and rarely quartz. These inclusions have homogenisation temperature between 1100 and 1060 °C and clearly display bimodal compositions: granitic Si-rich and ferrobasaltic Fe-rich. These inclusions clearly represent snapshots of trapped conjugate immiscible liquids.

Large-scale separation of these two immiscible melts is supported by the bimodal character of ferrogabbros. One group, enriched in plagioclase, has an average density of 3.0–3.2 g/cm^3 and contains 0–3.5 wt.% P_2O_5. The other group has an average density of 3.6–3.8 g/cm^3 with 3–12 wt.% P_2O_5. The two types of rocks have variable thicknesses and alternate at a scale of 5–20 m. The bimodality is interpreted to result from the segregation of the two immiscible melts, followed by crystallization and formation of two types of cumulates.

Layered Intrusions of the Emeishan Province

The 260 Ma Emeishan large igneous province in SW China host some major layered intrusions that are spatially and temporally associated with flood basalts and granitoids in the province (Zhou et al. 2008; Pang et al. 2010). They occur in the Panzhihua-Xichang (Panxi) region, and four of them host world-class resources of Fe, Ti and V: Panzhihua, Hongge, Baima and Xinjie (Pang et al. 2010).

Parental magmas to these intrusions are Fe–Ti-enriched basalts. Although Fe–Ti oxides saturate early in these basalts (Pang et al. 2008a), silicate liquid immiscibility has been invoked to explain the origin of the huge amounts of Fe–Ti-ores (Zhou et al. 2005). In this model, the separation of an immiscible oxide melts would be responsible for the formation of Fe–Ti–V oxide ore bodies in the lower part of the intrusion. Unmixing would have been triggered by the addition of fluids from upper crustal wall-rocks (Zhou et al. 2005). This model is supported by textural and mineralogical constraints from Hongge Fe–Ti–V oxide deposit showing the presence of two populations of Cr-rich and Cr-poor titanomagnetite (Wang and Zhou 2013). Cr-rich titanomagnetite is interpreted as an early liquidus phase whereas clusters of Cr-poor titanomagnetite, ilmenite, and apatite are thought to have formed from an Fe–Ti–(P)-rich immiscible melt. Ultimately, large-scale silicate liquid immiscibility in the region would be responsible for the formation of contrasting suites of rocks, with Si-rich immiscible melts forming syenites and Fe-rich immiscible melts crystallizing layered gabbros and massive oxides (Zhou et al. 2008).

Alternative models invoking continuous fractional crystallization have also been proposed. In this scenario, formation of huge amounts of Fe–Ti oxide is a simple result of gravitational sorting and settling (Pang et al. 2008b; Zhang et al. 2012). Frequent Fe–Ti-rich magma replenishment (Song et al. 2013) is coupled to sorting and settling to explain the formation of unusually thick stratiform Fe–Ti oxide layers.

Bushveld

The Paleoproterozoic (2054.4 ± 1.3 Ma; Scoates and Friedman 2008) Bushveld Complex in South Africa is a gigantic plutonic system comprising an inwardly dipping lopolith of mafic-ultramafic cumulate rocks, the Rustenburg Layered Suite (RLS), overlain in the centre by a large mass of contemporaneous granites. In terms of the total volume of basaltic magma, the Bushveld Complex by itself constitutes a large igneous province, with the intrusive equivalent of continental flood basalts. Present-day outcrops of the complex cover a surface area of 66,000 km^2 and the total thickness of igneous rocks is about 10 km or more. The mafic-ultramafic layered intrusion is sub-divided into stratigraphic zones comprising from the bottom to the top the Lower Zone (pyroxenites and harzburgites), Critical Zone (chromitites, harzburgites, pyroxenites, norites and minor anorthosites), Main Zone (norites and gabbronorites), and Upper Zone (gabbronorites and augite diorites). There is abundant evidence that the cumulates formed in an open system with multiple magma injections, volcanic eruptions and significant assimilation of continental crust. The open-system nature of magma evolution is evidenced in the RLS by trace element variations, breaks in initial Sr isotope ratios, and numerous reversals in compositional trends of cumulate minerals (Eales and Cawthorn 1996; Maier et al. 2013 and references therein). Studies of the chilled margins (Wilson 2012) and comagmatic sills associated with the RLS (Barnes et al. 2010) have revealed at least three distinct geochemical types of parental magmas. Recent studies of the Bushveld Complex are reviewed by Cawthorn (2015).

Silicate liquid immiscibility in the Bushveld Igneous Complex has been discussed in the context of magma differentiation in the Upper Zone including the origin of magnetite and nelsonite layers (e.g., Reynolds 1985; von Grunewaldt 1993) and especially in connection with the origin of iron-rich ultramafic pegmatites (IRUP). The latter are coarse-grained rocks forming distinct discordant bodies, ranging in size from a few meters to a few kilometers and randomly cutting through the layered rocks of the normal stratigraphy in the vertical interval from the Upper Zone down to the upper Critical Zone (Scoon and Mitchell 1994; Reid and Basson 2002). The bodies have irregular shapes resembling discs, tubes, sheets, dykes and complex branching forms (Fig. 5.12). Contacts with the host rocks are usually sharp and imply magmatic replacement reactions. Typical mineral assemblages of the IRUP comprise ferro-augite ($Wo_{34–46}En_{21–40}Fs_{18–40}$), olivine ($Fo_{30–50}$), magnetite, ilmenite and little or no plagioclase. Sulfides, Fe-amphibole and apatite may be locally abundant.

A genetic link between IRUP and silicate liquid immiscibility has been proposed primarily because typical whole-rock compositions of IRUP are high in FeOt, low in Al_2O_3 and resemble the compositions of Fe-rich immiscible melts (Scoon and Mitchell 1994; Reid and Basson 2002). Unmixing has been proposed to take place in parental magma of the Upper Zone because the initial $^{87}Sr/^{86}Sr$ isotope ratios of the IRUP cutting through the Upper Critical and the Main Zones are significantly different from those of the country rocks and similar to the rocks of the Upper Zone (Scoon and Mitchell 1994; Reid and Basson 2002). An origin of the IRUP-forming

Fig. 5.12 Exposures of iron-rich ultramafic pegmatites (IRUP; *dark*) replacing host leuconorite (*light*) in the U2 open pit of the Lonmin Marikana mine, Bushveld Complex (photo by DL Reid)

liquids in the parental magma of the Upper Zone is further supported by the Nd isotope data, Mg# of the Fe–Mg silicates, and the presence of liquidus magnetite (Reid and Basson 2002). In the Upper Critical Zone, the IRUP preferentially replace anorthosites and norites but in fully developed cases pyroxenite and even chromitite layers are also affected. The replacement reactions result in (1) reverse zoning of plagioclase in the IRUP in contact with norite or anorthosite, and complete disappearance of plagioclase from the inner, central parts of the IRUP bodies; (2) the replacement of low-Ca pyroxene by ferro-augite and olivine; (3) the replacement of chromite by magnetite. The nature and the origin of the IRUP replacement bodies defy a simple explanation, and remain contentious. Immiscibility hypothesis has been favored by some researches; however, it does not give all the answers to the problems posed by IRUP. For example, if the source of IRUP-forming liquids was indeed in the Upper Zone, one has to explain how the melts penetrated downwards through the 3 km thick cumulate pile of the Main Zone without changing their radiogenic isotope ratios, and how the melts became under-saturated in plagioclase.

Tegner and Cawthorn (2010) argued that the tholeiitic parental magma of the Upper Zone, in contrast with the parental magmas of the Skaergaard and Sept Iles intrusions, contained less FeOt from the start and did not follow the trend of strong Fe enrichment. Nevertheless, they did not rule out immiscibility and immiscible origin for prominent magnetite and nelsonite (apatite-magnetite) layers, which mark the Upper Zone stratigraphy. Recently VanTongeren and Mathez (2012) interpreted a sharp, 3-fold increase of REE concentrations in cumulus apatite at the top of the Upper Zone as a result of large-scale silicate liquid immiscibility and argued that the uppermost 325 m of the cumulates crystallized from gravitationally separated layer of the silica-rich immiscible liquid. Cawthorn (2013) challenged that interpretation

and put forward an alternative model. He proposed that higher REE concentrations in the uppermost apatite were due to post-cumulus re-equilibration of apatite primocrysts with a greater amount of inter-cumulus liquid. According to his calculations, a change of the apatite-liquid mass ratio in cumulus mush from 0.5 to 0.09 would account for the 3-fold increase of the final REE concentrations in re-equilibrated apatite. In conclusion, evidence for complete gravitational separation of Fe-rich and silica-rich immiscible liquids in two major, macroscopic layers may be missing at Bushveld, as well as from other layered intrusions. However, as discussed below in Section "Intercumulus Crystallization and Liquid Immiscibility", liquid immiscibility in mafic layered intrusions does not need to form major, fully separated liquid layers dozens of hundreds meters in thickness in order to play a significant role in post-cumulus crystallization and material transport.

Other Layered Intrusions

In the Duluth layered intrusion (Minnesota, USA), Ripley et al. (1998) proposed that nelsonites and possibly oxide- and apatite-rich rocks were formed by liquid immiscibilty together with a sulfide melt. The authors suggest an important role of evolved ferrogabbroic melt produced during crystallization of tholeiitic magmas.

In the Bjerkreim-Sokndal layered intrusion, Norway, it has been suggested that immiscibility might have occured in the Transition Zone, between the Layered Series and the overlying silicic evolved rocks (Wilson and Overgaard 2005). Experiments have shown that mixtures of jotunite and quartz mangerite, the most common melt compositions associated with anorthosites, are indeed immiscible (Philpotts 1981). Alternatively, the Transition Zone cumulates have been interpreted as resulting from crystallization of a single magma (Duchesne et al. 1987; Duchesne and Wilmart 1997).

Evidence for coexisting Fe-rich and Si-rich melts have also been found in the Sudbury igneous complex in Canada. This intrusion crystallized from a melt sheet produced by a meteorite impact (Grieve et al. 1991). Bimodal compositions have been interpreted to result from emulsion of superheated norite and granophyre assemblages (Zieg and Marsh 2005). Melt inclusions trapped in apatite have preserved the composition of the two melts (Watts 2014), considered to be produced by immiscibility during cooling of the superheated melt sheet.

Loferski and Arculus (1993) described multiphase crystallized melt inclusions in cumulus plagioclase crystals from anorthosite layers and other rocks in the Middle Banded series of the Stillwater Complex (Monatana, USA) and interpreted the inclusions as traces of immiscible Fe-rich liquid concentrating Ti, P, Zr and REE. The authors proposed that silicate liquid immiscibility in Stillwater could either have occurred locally in compositional boundary layers around crystallizing plagioclase grains, or it could have occurred pervasively throughout the parent melt. Large masses of monomineral anorthosites may have crystallized from the main, feldspathic, silica-rich immiscible liquid.

Intercumulus Crystallization and Liquid Immiscibility

Despite disagreements about the exact timing of silicate liquid immiscibility in some specific cases, the broadly accepted view is that immiscibility in mafic layered intrusions starts at a late stage of magma evolution after extensive magma differentiation by fractional crystallization. The lowest temperatures and the most evolved melt fractions are likely to be found in partly crystallized marginal zones of a magma chamber, at the bottom, sides and at the roof. Therefore, unmixing is likely to start at first in intercumulus melt inside partly solidified crystal mush. If mush permeability is low and immiscible melts cannot separate by gravity, immiscibility will leave no traces in fully crystallized rocks. Both melts should crystallize identical mineral assemblages and crystallization products of a melt mixture would be indistinguishable from those of a single homogenous melt of the same bulk composition.

However, if the crystal mush is permeable enough for liquid-liquid fractionation by gravity, immiscibility would provide effective means of material transport in the form of phase convection and that may significantly affect intercumulus crystallization. Consider, for example, a section of gabbroic cumulus mush at the bottom of a magma chamber (Fig. 5.13). Suppose a vertical temperature gradient across the mush with the temperature increasing upwards. Suppose the porosity and permeability of the mush increase in the same direction. Part of the mush below the im-

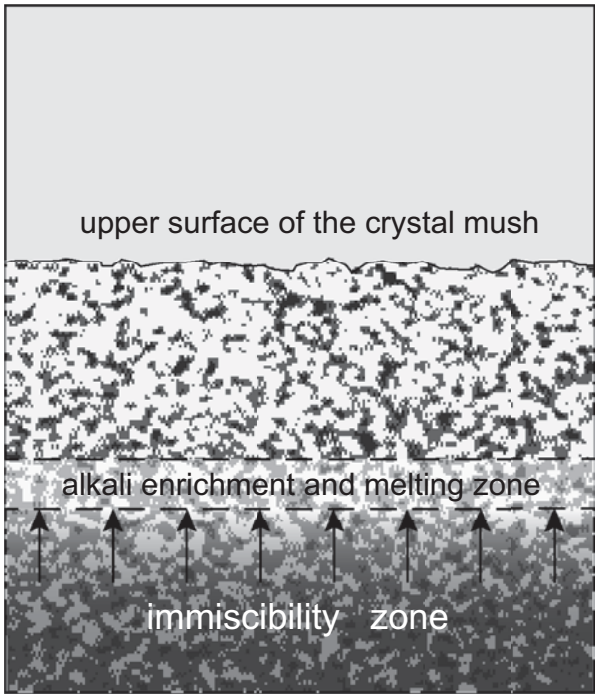

Fig. 5.13 Immiscibility in a cumulus crystal mush. See text for discussion

miscibility isotherm is labeled in Fig. 5.13 as immiscibility zone. Within the zone, immiscible melts are stable and separate by gravity. The lighter silica-rich melt moves upwards where it should eventually cross immiscibility isotherm, above which immiscibility is unstable. At this point, the immiscible silica-rich melt must re-dissolve in the resident intercumulus liquid. The dissolving melt brings extra silica and alkalis in the form of albite and orthoclase aluminosilicate components. The additions of such components to the multiply-saturated intercumulus melt are expected to trigger a series of crystal-melt reactions. For example, additional alkalis would offset the Ca/Na balance and the plagioclase-melt equilibrium. This should result in partial melting of cumulus plagioclase right above immiscibility zone. Pyroxenes and other minerals should also melt to keep the intercumulus liquid at equilibrium cotectic composition. Partial melting of earlier formed cumulates may have a positive feedback on the melt migration because of the increasing porosity and permeability in the melting zone. The extent of melting would depend on the balance between the cooling rate of the magma chamber and the rate of melt migration. Other factors, such as variations in melt viscosity or the size of immiscible melt droplets may also play significant roles. In principle, the process may lead to complete dissolution of some cumulus minerals and formation of monomineral layers. In any case, the consequences of intercumulus immiscibility appear to be complex and the effects of the resulting material transport may be far-reaching.

Conclusions and the Outlook

More and more evidence for immiscibility between two silicate melts in layered intrusions have been provided. Contrasted melt inclusions trapped in cumulus phases provide the most obvious record for the coexistence of equilibrium paired melts, as described in the Skaergaard and Sept Iles intrusions. The process affects the liquid line of descent during its late-stage evolution although the exact onset of unmixing is debated. Even if the two melts have contrasting physical properties (density, viscosity), their ability to segregate on large scale has still to be proven. Kinetics issues hamper nucleation and growth of immiscible droplets, so that small-scale segregation in the crystal mush might be more common than large-scale separation of the paired melts. The process has nevertheless implications for the formation of Fe–Ti–P ore deposits in layered intrusions, and by analogy, could also be important for the origin of Kiruna-type iron ore deposit. Further work might focus on the understanding of nucleation, growth, and potential segregation of immiscible melts.

Acknowledgments This paper has been reviewed by Jean Clair Duchesne and Jakob Klove Keiding. Olivier Namur is thanked for the editorial handling. BC acknowledges support by a Marie Curie International Outgoing Fellowship within the 7th European Community Framework Programme. IVV has been supported by the German Science Foundation (DFG) grants FR 557/23-2 and VE 619/2-1, and the Russian Science Foundation (RNF) grant No. 14-17-00200.

References

Barnes S-J, Maier WD, Curl EA (2010) Composition of the marginal rocks and sills of the Rustenburg Layered Suite, Bushveld Complex, South Africa: implications for the formation of the platimum-group element deposits. Econ Geol 105:1491–1511

Bogaerts M, Schmidt MW (2006) Experiments on silicate melt immiscibility in the system Fe_2SiO_4–$KAlSi_3O_8$–SiO_2–CaO–MgO–TiO_2–P_2O_5 and implications for natural magmas. Contrib Mineral Petrol 152: 257–274

Bowen NL (1928) The evolution of the igneous rocks. Princeton University Press, Princeton, p 332

Brooks CK, Nielsen TFD (1990) The differentiation of the Skaergaard intrusion. A discussion of Hunter and Sparks (Contrib Mineral Petrol 95:451–461). Contrib Mineral Petrol 104:244–247

Cawthorn RG (2013) Rare earth element abundances in apatite in the Bushveld Complex—A consequence of the trapped liquid shift effect. Geology 41:603–606

Cawthorn RG (2015) The Bushveld Complex, South Africa. In: Charlier B et al (eds) Layered Intrusions. Springer, Heidelberg

Charlier B, Grove TL (2012) Experiments on liquid immiscibility along tholeiitic liquid lines of descent. Contrib Mineral Petrol 164:27–44

Charlier B, Namur O, Toplis MJ, Schiano P, Cluzel N, Higgins MD, Vander Auwera J (2011) Large-scale silicate liquid immiscibility during differentiation of tholeiitic basalt to granite and the origin of the Daly gap. Geology 39:907–910

Charlier B, Namur O, Grove TL (2013) Compositional and kinetic controls on liquid immiscibility in ferrobasalt-rhyolite volcanic and plutonic series. Geochim Cosmochim Acta 113(0):79–93

Chayes F (1963) Relative abundance of intermediate members of the oceanic basalt-trachyte association. J Geophys Res 68(5):1519–1534

Daly RA (1914) Igneous rocks and their origin. McGraw-Hill, NewYork, p 563

De A (1974) Silicate liquid immiscibility in the Deccan traps and its petrogenetic significance. Geol Soc Am Bull 85:471–474

Dixon S, Rutherford MJ (1979) Plagiogranites as late-stage immiscible liquids in ophiolite and mid-ocean ridge suites: an experimental study. Earth Planet Sci Lett 45(1):45–60

Doremus RH (1994) Glass science. Wiley and, New York

Duchesne JC (1999) Fe–Ti deposits in Rogland anorthosites (South Norway): geochemical characteristics and problems of interpretation. Miner Depos 34:182–198

Duchesne JC, Wilmart E (1997) Igneous charnokites and related rocks from the Bjerkreim-Sokndal layered intrusion (Southwest Norway): a jotunite (hyperstene monzodiorite)-derived A-type granitoide suite. J Petrol 38:337–369

Duchesne JC, Denoiseux B, Hertogen J (1987) The norite-mangerite relationships in the Bjerkreim-Sokndal layered lopolith (SW Norway). Lithos 20:1–17

Eales HV, Cawthorn RG (1996) The Bushveld Complex. In: Cawthorn RG (ed) Layered intrusions. Elsevier, Amsterdam, pp 181–229

Freestone IC Hamilton DL (1977) Liquid immiscibility in K_2O–FeO–Al_2O_3–SiO_2: discussion. Nature 267:559

Greig JW (1927) Immiscibility in silicate melts. Am J Sci 13:133–154

Grieve RAF, Stöffler D, Deutsch A (1991) The Sudbury structure: Controversial or misunderstood? J Geophys Res Planets 96(E5):22753–22764

Hess PC (1995) Thermodynamic mixing properties and the structure of silicate melts. In: Stebbins JF, McMillan PF, Dingwell DB (eds) Structure, dynamics and properties of silicate melts. Mineral Soc America, Washington, DC Rev Miner 32:145–190

Hess PC (1996) Upper and lower critical points: Thermodynamic constraints on the solution properties of silicate melts. Geochim Cosmochim Acta 60:2365–2377

Higgins MD (2005) A new interpretation of the structure of the Sept Iles Intrusive suite, Canada. Lithos 83(3–4):199–213

Holness MB, Stripp G, Humphreys MCS, Veksler IV, Nielsen TFD (2011) Silicate liquid immiscibility within the crystal mush: Late-stage magmatic microstructures in the Skaergaard Intrusion, East Greenland. J Petrol 52:175–222

Hoover JD, Irvine TN (1978) Liquidus relations and Mg–Fe partitioning on part of the system Mg_2SiO_4–Fe_2SiO_4–$CaMgSi_2O_6$–$CaFeSi_2O_6$–$KAlSi_3O_8$–SiO_2. Carnegie Inst Wash Yearb 77, 774–784

Hou T, Zang Z, Kusky T (2011) Gushan magnetite-apatite deposit in the Ningwu basin, lower Yangtze River Valley, SE China: hydrothermal or Kiruna-type? Ore Geol Rev 33:333–346

Hudon P, Baker DR (2002) The nature of phase separation in binary oxide melts and glasses. I. silicate systems. J Non-Cryst Solids 303:299–345

Humphreys MCS (2011) Silicate liquid immiscibility within the crystal mush: evidence from Ti in plagioclase from the Skaergaard intrusion. J Petrol 52:147–174

Hunter RH, Sparks RSJ (1987) The differentiation of the Skaergaard intrusion. Contrib Mineral Petrol 95:451–461

Hunter RH, Sparks RSJ (1990) The differentiation of the Skaergaard intrusion. A reply. Contrib Mineral Petrol 104:248–254

Jakobsen JK, Veksler IV, Tegner C, Brooks CK (2005) Immiscible iron- and silica-rich melts in basalt petrogenesis documented in the Skaergaard intrusion. Geology 33:885–888

Jakobsen JK, Veksler IV, Tegner C, Brooks CK (2011) Crystallization of the Skaergaard intrusion from an emulsion of immiscible iron- and silica-rich liquids: evidence from melt inclusions in plagioclase. J Petrol 52: 345–373

James PF (1975) Liquid-phase separation in glass-forming systems. J Mater Sci 10:1802–1825

Juster TC, Grove TL, Perfit MR (1989) Experimental constraints on the generation of FeTi basalts, andesites, and rhyodacites at the Galapagos spreading center, 85°W and 95°W. J Geophys Res 94(B7):9251–9274

Kolker A (1982) Mineralogy and geochemistry of Fe–Ti oxides and apatite (nelsonite) deposits and evaluation of the liquid immiscibility hypothesis. Econom Geol 77:1146–1158

Kontak DJ, De Wolfe De Young MY, Dostal J (2002) Late-stage crystallization history of the Jurassic North Mountain Basalt, Nova Scotia, Canada. I. Textural and chemical evidence for pervasive development of silicate-liquid immiscibility. Can Miner 40:1287–1311

Kyser TK, Lesher CE, Walker D (1998) The effects of liquid immiscibility and thermal diffusion on oxygen isotopes in silicate liquids. Contrib Mineral Petrol 133:373–381

Lester GW, Clark AH, Kyser TK, Naslund HR (2013a) Experiments on liquid immiscibility in silicate melts with H_2O, P, S, F, and Cl: implications for natural magmas. Contrib Mineral Petrol 166:329–349

Lester GW, Kyser TK, Clark AH (2013b) Oxygen isotope partitioning between immiscible silicate melts with H_2O, P and S. Geochim Cosmochim Acta 109:306–311

Levin EM, Robbins CR, McMurdie HF (1964) Phase Equilibria Diagrams, vol 1. American Ceramic Society, Westerville

Loferski PJ, Arculus RJ (1993) Multiphase inclusions in plagioclase from anorthosites in the Stillwater Complex, Montana: implications for the origin of the anorthosites. Contrib Mineral Petrol 114:63–78

Longhi J (1998) Silicate liquid immiscibility: a furtive agent of fractionation. 29th Lunar and Planetary Science Conference, abstract No 1903

Maier WD, Barnes S-J, Groves DI (2013) The Bushveld Complex, South Africa: formation of platinum-palladium, chrome- and vanadium-rich layers via hydrodynamic sorting of a mobilized cumulate slurry in a large, relatively slowly cooling, subsiding magma chamber. Miner Depos 48(1):1–56

Martin B, Kushiro Y (1991) Immiscibility synthesis as an indicator of cooling rates in basalts. J Volcanol Geotherm Res 45:289–310

Mazurin OV, Porai-Koshits EA (1984) Phase separation in glass. Amsterdam, North-Holland, p 382

McBirney AR (1996) The Skaergaard intrusion. In: Cawthorn RG (ed) Layered intrusions. Developments in Petrology, 15. Elsevier, Amsterdam, pp 147–180

McBirney AR (2008) Comments on: 'liquid Immiscibility and the Evolution of Basaltic Magma'. J Petrol 48:2187–2210, 49:2169–2170

McBirney AR, Nakamura Y (1974) Immiscibility in late-stage magmas of the Skaergaard intrusion. Carnegie Inst Wash Yearb 73:348–352
McBirney AR, Naslund HR (1990) The differentiation of the Skaergaard intrusion. A discussion of Hunter and Sparks (Contrib Mineral Petrol 95:451–461). Contrib Mineral Petrol 104:235–240
Morse SA (1990) The differentiation of the Skaergaard intrusion. A discussion of Hunter and Sparks (Contrib Mineral Petrol 95:451–461). Contrib Mineral Petrol 104:240–244
Morse SA (2008) Compositional convection trumps silicate liquid immiscibilty in layered intrusions: a discussion of 'Liquid immiscibility and the evolution of basaltic magma' by Veksler et al. J Petrol 48:2187–2210, 49:2157–2168
Namur O, Charlier B, Toplis MJ, Higgins MD, Liégeois J-P, Vander Auwera J (2010) Crystallization sequence and magma chamber processes in the ferrobasaltic Sept Iles layered intrusion, Canada. J Petrol 51:1203–1236
Namur O, Charlier B, Toplis MJ, Higgins MD, Hounsell V, Liégeois JP, Vander Auwera J (2011) Differentiation of tholeiitic basalt to A-type granite in the Sept Iles layered intrusion, Canada. J Petrol 52:487–539
Namur O, Charlier B, Holness MB (2012) Dual origin of Fe–Ti–P gabbros by immiscibility and fractional crystallization of evolved tholeiitic basalts in the Sept Iles layered intrusion. Lithos 154(0):100–114
Namur O, Higgins MD, Vander Auwera J (2015) The Sept Iles intrusive suite, Quebec, Canada. In Charlier B et al (eds) Layered intrusions. Springer, Heidelberg
Navrotsky A (1992) Unmixing of hot inorganic melts. Nature 360:306
Nielsen TFD (2004) The shape and volume of the Skaergaard intrusion, Greenland: implications for mass balance and bulk composition. J Petrol 45:507–530
Pang K-N, Li C, Zhou M-F, Ripley EM (2008a) Abundant Fe–Ti oxide inclusions in olivine from the Panzhihua and Hongge layered intrusions, SW China: evidence for early saturation of Fe–Ti oxides in ferrobasaltic magma. Contrib Mineral Petrol 156:307–321
Pang KN, Zhou MF, Lindsley D, Zhao D, Malpas J (2008b) Origin of Fe–Ti oxide ores in mafic intrusions: Evidence from the Panzhihua intrusion, SW China. J Petrol 49:295–313
Pang KN, Zhou MF, Qi L, Shellnutt G, Wang CY, Zhao D (2010) Flood basalt-related Fe–Ti oxide deposits in the Emeishan large igneous province, SW China. Lithos 119(1–2):123–136
Philpotts AR (1967) Origin of certain iron-titanium oxide and apatite rocks. Econ Geol 62:303–315
Philpotts AR (1979) Silicate liquid immiscibility in tholeiitic basalts. J Petrol 20:99–118
Philpotts AR (1981) A model for the generation of massif-type anorthosites. Can Miner 19:233–253
Philpotts AR (1982) Compositions of immiscible liquids in volcanic rocks. Contrib Mineral Petrol 80:201–218
Philpotts AR (2008) Comments on: Liquid immiscibility and the evolution of basaltic magma. J Petrol 49:2171–2175
Philpotts AR, Doyle CD (1983) Effect of magma oxidation state on the extent of silicate liquid immiscibility in a tholeiitic basalt. Am J Sci 283(9):967–986
Powell MA, Walker D, Hays JF (1980) Controlled cooling and crystallization of a eucrite: Microprobe studies. Proc Lunar Planet Sci Conf 11th 2:1153–1168
Reid DL, Basson IJ (2002) Iron-rich ultramafic pegmatite replacement bodies within the upper critical zone, Rustenburg layered suite, Northam Platinum Mine, South Africa. Miner Mag 66:895–914
Reynolds IM (1985) The nature and origin of titaniferous magnetite-rich layers in the upper zone of the Bushveld Complex: a review and synthesis. Econ Geol 80:1089–1108
Ripley EM, Severson MJ, Hauck SA (1998) Evidence for sulfide and Fe–Ti–P-rich liquid immiscibility in the Duluth Complex, Minnesota. Econ Geol 93(7):1052–1062
Roedder E (1951) Low-temperature liquid immiscibility in the system K_2O–FeO–Al_2O_3–SiO_2. Am Miner 36:282–286
Roedder E (1978) Silicate liquid immiscibility in magmas and in the system K_2O–FeO–Al_2O_3–SiO_2: an example of serendipity. Geochim Cosmochim Acta 43:1597–1617

Roedder E (1979) Silicate liquid immiscibility in magmas. In: Yoder HS Jr (ed) The evolution of igneous rocks. Fiftieth Anniversary perspectives. Princeton University Press, Princeton, pp 15–58

Rutherford MJ, Hess PC, Daniel GH (1974) Experimental liquid line of descent and liquid immiscibility for basalt 70017. Proc Proceedings of the 5th Lunar Science Conference, pp 569–583

Sato H (1978) Segregation vesicles and immiscible liquid droplets in ocean-floor basalt of Hole 396B, IPOD/DSDP Leg 46. In: Dimitriev L, Heirtzler J (eds) Initial reports of the deep sea drilling project v 46, U.S. Gov Printing Office, Washington, pp 283–291

Schmidt MW Connolly JAD, Günther D, Bogaerts M (2006) Element partitioning—the role of melt structure and composition. Science 312:1646–1650

Scoates JS, Friedman RM (2008) Precise age of the platiniferous Merensky Reef, Bushveld Complex, South Africa, by the U–Pb zircon chemical ID-TIMS abrasion technique. Econ Geol 103:465–471

Scoon RN, Mitchell AA (1994) Discordant iron-rich ultramafic pegmatites in the Bushveld Complex and their relationship to iron-rich intercumulus and residual liquids. J Petrol 35:881–917

Sensarma S, Palme H (2013) Silicate liquid immiscibility in the ~2.5 Ga Fe-rich andesite at the top of the Dongargarh large igneous province (India). Lithos 170–171:239–251

Shelby JE (2005) Introduction to glass science and technology. The Royal Society of Chemistry, Cambridge

Simmons JH, Macedo PB (1971) Analysis of viscous relaxation in critical oxide mixtures. J Chem Phys 54:1325–1331

Simmons JH, Napolitano A, Macedo PB (1970) Supercritical viscosity anomaly in oxide mixtures. J Chem Phys 53:1165–1170

Song XY, Qi HW, Hu RZ, Chen LM, Yu SY, Zhang JF (2013) Formation of thick stratiform Fe–Ti oxide layers in layered intrusion and frequent replenishment of fractionated mafic magma: evidence from the Panzhihua intrusion, SW China. Geochem Geophys Geosyst 14(3):712–732

Tegner C, Cawthorn RG (2010) Iron in plagioclase in the Bushveld and Skaergaard intrusions: implications for iron contents in evolving basic magmas. Contrib Mineral Petrol 159:719–730

Thompson RN (1972) Evidence for a chemical discontinuity near the basalt-andesite transition in many anorogenic volcanic suites. Nature 236(5342):106–110

Thompson AB, Aerts M, Hack AC (2007) Liquid immiscibility in silicate melts and related systems. Rev Mineral Geochem 65:99–127 (In: Liebscher A, Heinrich CA (eds) Fluid-fluid interactions)

Thy P, Lesher CE, Nielsen TFD, Brooks CK (2006) Experimental constraints on the Skaergaard liquid line of descent. Lithos 92:154–180

Toplis MJ, Carroll MR (1995) An experimental study of the influence of oxygen fugacity on Fe–Ti oxide stability, phase relations, and mineral-melt equilibria in ferro-basaltic systems. J Petrol 36:1137–1171

VanTongeren JA, Mathez EA (2012) Large-scale liquid immiscibility at the top of the Bushveld Complex, South Africa. Geology 40:491–494

Veksler IV (2004) Liquid immiscibility and its role at the magmatic-hydrothermal transition: a summary of experimental studies. Chem Geol 210:7–31

Veksler IV (2009) Extreme iron enrichment and liquid immiscibility in mafic intrusions: experimental evidence revisited. Lithos 111:72–82

Veksler IV, Dorfman AM, Danyushevsky LV, Jakobsen JK, Dingwell DB (2006) Immiscible silicate liquid partition coefficients: Implications for crystal-melt element partitioning and basalt petrogenesis. Contrib Mineral Petrol 152:685–702

Veksler IV, Dorfman AM, Borisov AA, Wirth R, Dingwell DB (2007) Liquid immiscibility and evolution of basaltic magma. J Petrol 48:2187–2210

Veksler IV, Dorfman AM, Rhede D, Wirth R., Borisov AA, Dingwell DB (2008a) Kinetics and the extent of liquid immiscibility in the system K_2O–CaO–FeO–Al_2O_3–SiO_2. Chem Geol 256:119–130

Veksler IV, Dorfman AM, Borisov AA, Wirth R, Dingwell DB (2008b) Liquid immiscibility and evolution of basaltic magma. Reply to SA Morse, AR McBirney and AR Philpotts. J Petrol 49:2177–2186

Veksler IV, Kähn J, Franz G, Dingwell DB (2010) Interfacial tension between immiscible liquids in the system K_2O–FeO–Fe_2O_3–Al_2O_3–SiO_2 and implications for the kinetics of silicate melt unmixing. Am Miner 95:1679–1685

Visser W, Koster van Groos AF (1976) Liquid immiscibility in K_2O–FeO–Al_2O_3–SiO_2. Nature 264:426–427

Visser W, Koster van Groos AF (1977) Liquid immiscibility in K_2O–FeO–Al_2O_3–SiO_2: reply to Roedder, Freestone and Hamilton. Nature 267:560

Visser W, Koster van Groos AF (1979) Phase relations in the system K_2O–FeO–Al_2O_3–SiO_2 at 1 atmosphere with special emphasis on low temperature liquid immiscibility. Am J Sci 279:70–91

von Gruenewaldt G (1993) Ilmenite-apatite enrichments in the upper zone of the Bushveld Complex: a major titanium-rock phosphate resource. Int Geol Rev 35: 987–1000

Wager LR, Deer WA (1939) Geological investigation in East Greenland, Part III, The petrology of the Skaergaard intrusion, Kangerdluqssuaq, East Greenland. Meddelser om Grønland 105(4)283–296

Wang C, Zhou MF (2013) New textural and mineralogical constraints on the origin of the Hongge Fe–Ti–V oxide deposit, SW China. Miner Depos 48:787–798

Watts K (2014) A melt inclusion study of the Sudbury Igneous Complex (Ontario, Canada): evidence for two-liquid immiscibility and constraints on trace element distribution. Master Thesis, Saint Mary's University, Halifax, p 129

Wilson AH (2012) A chill sequence to the Bushveld Complex: insight into the first stage of magma emplacement and implications for parental magmas. J Petrol 53:1123–1168

Wilson JR, Overgaard G (2005) Relationship between the layered series and the overlying evolved rocks in the Bjerkreim-Sokndal intrusion, Southern Norway. Lithos 83(3–4):277–298

Zhang XQ, Song XY, Chen LM, Xie W, Yu SY, Zheng WQ, Deng YF, Zhang JF, Gui SG (2012) Fractional crystallization and the formation of thick Fe–Ti–V oxide layers in the Baima layered intrusion, SW China. Ore Geol Rev 49:96–108

Zhou M-F, Robinson PT, Lesher CM, Keays RR, Zhang C-J, Malpas J (2005) Geochemistry, petrogenesis and metallogenesis of the Panzhihua gabbroic layered intrusion and associated Fe–Ti–V oxide deposits, Sichuan Province, SW China. J Petrol 46:2253–2280

Zhou M-F, Arndt NT, Malpas J, Wang CY, Kennedy AK (2008) Two magma series and associated ore deposit types in the Permian Emeishan large igneous province, SW China. Lithos 103:352–368

Zieg MJ, Marsh BD (2005) The Sudbury Igneous Complex: viscous emulsion differentiation of a superheated impact melt sheet. Geol Soc Am Bull 117(11–12):1427–1450